ACS Synthetic Biology
Cite This: ACS Synth. Biol. 2018, 7, 1829−1833
Letter
pubs.acs.org/synthbio

Electric-Field Manipulation of a Compartmentalized Cell-Free Gene Expression Reaction

Yuval Efrat,[†] Alexandra M. Tayar,[†] Shirley S. Daube, Michael Levy, and Roy H. Bar-Ziv*

Department of Chemical and Biological Physics, Weizmann Institute of Science, Rehovot 7610001, Israel

Supporting Information

ABSTRACT: Direct electric-field manipulation of gene expression reactions would simplify the design of biochemical networks by replacing complex biomolecular interactions with push-button operations. Here, we applied a localized electric field gradient at megahertz frequency to manipulate a cell-free gene-expression reaction in a DNA compartment on a chip. We broke the spatial symmetry of a homogeneous reaction in the compartment by creating a trap for macromolecules in a region of maximal field intensity localized 50 μm from immobilized DNA. Free of biochemical regulation, we demonstrated protein synthesis oscillations by on/off switching of the electric field. In response to the field, ribosomes, RNA polymerases, and nascent RNA and proteins accumulated in the trap, and were then depleted from the DNA region where gene expression occurred. The resulting reduction in the rate of protein synthesis recovered back to steady-state when the field was off. The combination of electric field with compartmentalized cell-free gene expression reactions creates a simple, label-free approach for controlling biomolecules in space and time, opening possibilities for hybrid biological systems with a bioelectronic interface based on minimal biological parts design.

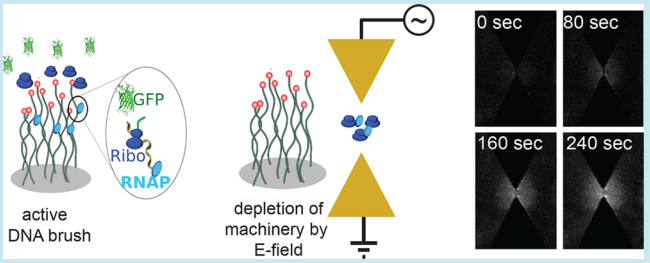

Cellular complexity is governed by patterns of proteins that change in space and time. Recreating such patterns in cells or in a cell-free synthetic framework requires programming molecular interactions to regulate gene-expression reaction networks,[1−4] including recent effort toward a bioelectronic interface.[5] The number of biological components that must be integrated scales up with the complexity of the network.[6,7] Biomolecular synthetic design would be simplified if molecular regulation of gene expression were replaced by external-field manipulation. Control of biochemical reactions by external fields can be achieved by light,[8−10] magnetic field[11,12] and electrochemical transduction,[13,14] yet these have so far required tailored responsive molecules and nanoparticles. Without auxiliary molecular mediators, heating can directly affect gene expression from anchored genes.[15] Temperature gradients combined with convection provide a means to spatially compartmentalize biochemical reactions,[16] yet temperature has a global effect on all reaction rates.

Electric-field (E-field) manipulation of biochemical reactions could in principle be more specific, rapid, and combined with microelectronics. However, to manipulate by E-field a gene-expression reaction, which occurs at physiologically relevant conditions, we must overcome the ionic Debye electrostatic screening, and avoid detrimental effects of currents flowing in the solution.[17] To this end, we chose to use dielectrophoresis (DEP) to polarize and trap biomolecules under a nonuniform E-field at a high frequency above the diffusion rate of ions.[18] Various forms of DEP have recently been applied to trap, manipulate and separate biomolecules with important technological applications.[19−21] The force acting on a biomolecule is proportional to its induced polarizability, α, attracting it toward regions of highest E-field gradients, $F_{DEP} = \frac{1}{2}\alpha\nabla E^2$. This effect decays in space as, $F_{DEP} \sim \alpha V^2/d^3$, where d is the typical decay length of the E-field gradient, and V the applied voltage. The E-field also induces Joule heating in the conductive solution, which leads to longer-range electrothermal flow beyond the DEP force.[22−25]

To study the response of gene expression to an E-field we used a reconstituted cell-free protein synthesis reaction based on purified components[26] (PURE system). Cell-free systems[26−28] provide a means to study biological design principles by programming minimal gene networks to exhibit emergent spatiotemporal expression patterns.[3,4,29−31] To overcome the challenge of manipulating homogeneously dispersed reaction components, we immobilized the DNA code as a dense brush, thereby breaking the symmetry and localizing the reaction close to the surface of a compartment. An E-field gradient applied to electrodes patterned close to the DNA brush creates a scenario for effectively perturbing the reaction by separating transcription-translation enzymes from the DNA code. At megahertz frequency we overcome screening and electro-osmotic effects in a solution of high ionic strength[17,32] with conductivity of about ∼1 S/m.

We assembled the DNA compartment as an artificial cell[3] by carving in silicon two overlapping circles of radius R = 35 μm and depth of h = 3 μm, which were connected to a large feeding channel through a capillary of width W = 15 μm and

Received: April 12, 2018
Published: July 23, 2018

DOI: 10.1021/acssynbio.8b00160
ACS Synth. Biol. 2018, 7, 1829−1833

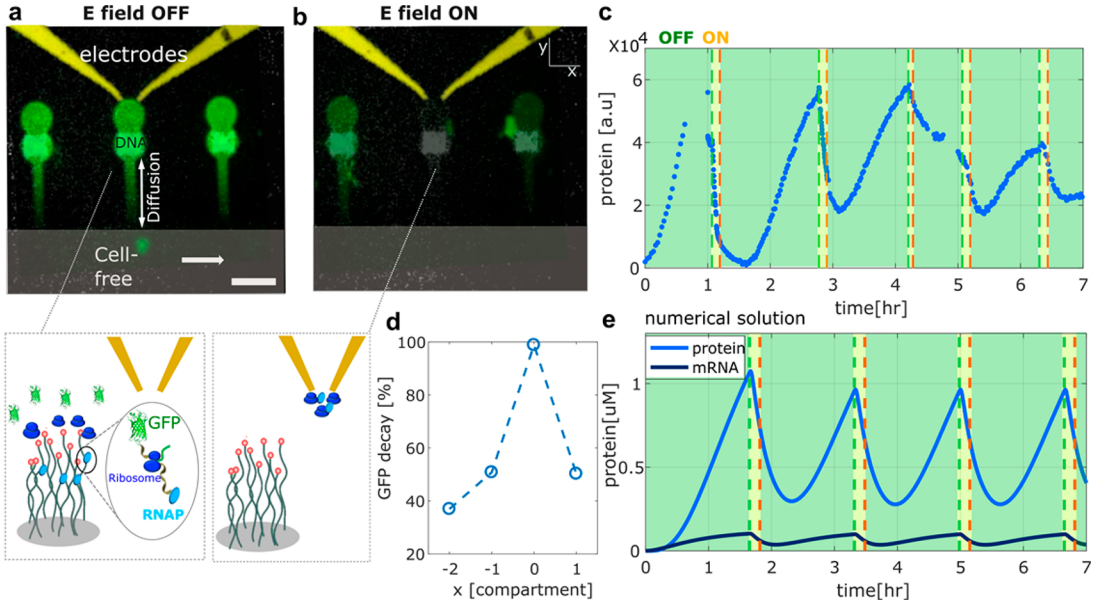

Figure 1. Electric-field manipulation of gene expression in a DNA compartment. (a) E-field OFF: GFP expression in silicon compartments overlaid with image of fluorescently labeled DNA coding for GFP under T7 promoter (square pattern in bottom compartments). The direction of flow of cell-free PURE reaction is shown (white arrow). Only the central top compartment was connected to gold electrodes (yellow). (b) E-field ON: Same imaging upon application of E-field to electrodes at 1 MHz, 10 V_{pp}. Scale bar: 100 μm. Schemes: RNAP (light blue) and ribosomes (dark blue) are localized to the DNA brush when E-field is OFF but attracted to electrodes and depleted from the DNA brush when E field is ON. (c) Periodic pulses of protein synthesis driven by E-field for a duration of 5 min each, with third pulse at 10 MHz, 10 V_{pp}; E-field ON (green marks), E-field OFF (red marks). (d) Decay of GFP expression measured in DNA compartments as a function of distance from electrodes. (e) Numerical solution of kinetics of gene expression reaction in the compartment taking into account depletion of both RNAP and ribosome (eqs S1−4).

length L = 200 μm (Figures 1a and S1). The entire chip was coated with a 50 nm thin SiO_2 insulating layer, and two gold electrodes, 100 nm thin and d = 15 μm apart, were evaporated on the upper surface of the chip at the upper compartment. The chip was then coated by a photoactivable monolayer, and linear DNA templates coding for GFP under a T7 promoter were patterned in the lower compartment. Once the chip was sealed, a PURE reaction was flown in the feeding channel, diffused into the compartment to initiate mRNA transcription and protein synthesis. Continuous expression in the compartment and dilution of products out of the capillary maintained protein concentration at steady-state. The effective protein lifetime in the compartment was set by geometry and diffusion, $\tau = \frac{2\pi R^2 L}{DW} \approx 45$ min, with D = 45 $\mu m^2/s$ the diffusion coefficient of GFP.[3]

We applied an AC electric potential of 10 V_{pp} at 1 MHz frequency between the electrodes connected to the DNA compartment, for a duration of 5 min. Upon application of the E-field, GFP concentration immediately dropped and continuously decreased, reaching zero value within 20 min (Figure 1b,c). GFP levels then gradually increased again at a rate comparable to the initial synthesis rate and continued for 60 min before another E-field application. This process was then repeated 4 times, creating E-field driven periodic pulses in protein concentration (Figure 1c). The recovery time matched the compartment lifetime, τ, suggesting that complete depletion of machinery and products occurred throughout the E-field ON period (Figure 1b,c). Notably, the effect of E-field on gene expression was most pronounced in the compartment connected to the electrodes, and could be observed to a lesser extent as a function of distance of nearby compartments (Figure 1d). The DNA remained intact and bound to the surface throughout the experiment.

To explain the effect of the E-field in the compartment, we examined a scenario in which a pulse of DEP stops protein synthesis by depletion of biomolecules involved in the reaction, including T7 RNA polymerase (RNAP) and ribosomes, the enzymatic machineries that synthesize the respective mRNA and GFP products. A numerical solution to a transcription-translation coupled differential eqs (eq S1−4), indicated that depletion of RNAP and ribosomes sufficiently captures the salient features of the dynamics (Figure 1e, S2): (i) immediate drop in GFP concentration upon E-field application and rapid decrease due to machinery depletion within a few minutes; (ii) further drop in GFP after inactivation of E-field; (iii) slower recovery of GFP synthesis due to replenishment of machinery by diffusion from the capillary, over a time scale of τ. The simulation also indicated that depletion of GFP, rather than machinery, cannot by itself reproduce the lag in recovery after inactivation of E-field (Figure S2). The direction of the E-field gradient in the compartment was simulated as well, and was found to be consistent with attraction of biomolecules toward the region of highest field intensity close to the electrodes (Figure S3).

To better understand the effect of E-field in the DNA compartment we sought to directly measure the response of the key molecular components in a larger chamber, 250 μm deep and 3 mm wide, with electrodes d = 10 μm apart on a fused silica insulating surface (Figure 2a). The DEP force field perpendicular to the E-field was visualized by the streamlines of 1 μm beads in water, where the Joule heating and electro-osmosis at high ionic strength[32] is minimized, leaving DEP as the main effect driving bead motion[33] (Figures 2b, S4). The attraction of the beads to the maximal field intensity region between the electrodes is consistent with a numerical solution of the DEP force field (Figure S5). Next, we carried out separate PURE protein-synthesis reactions, each supplemented

DOI: 10.1021/acssynbio.8b00160
ACS Synth. Biol. 2018, 7, 1829−1833

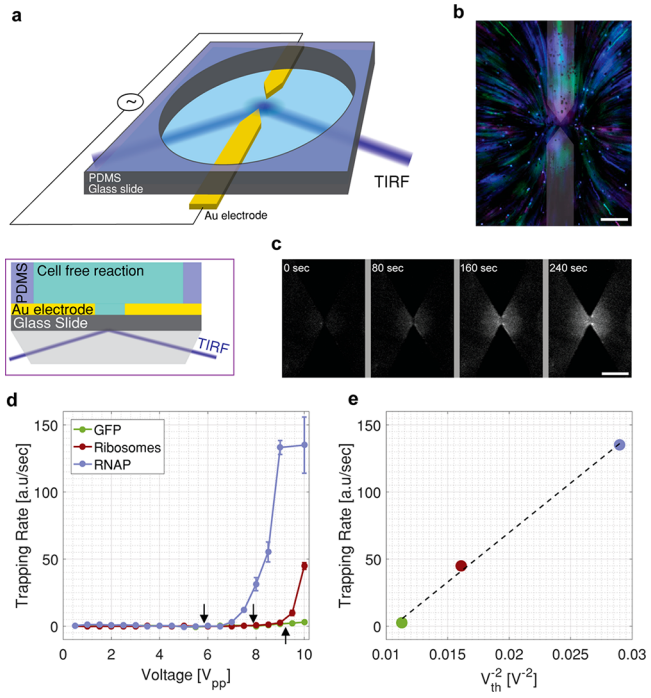

Figure 2. TIRF measurement of biomolecular trapping near electrodes. (a) Scheme: gold electrodes patterned on fused silica coverslip (100 nm, yellow) embedded in a circular PDMS chamber (250 μm thickness, 3 mm diameter), and mounted on a prism for detection of biomolecular localization close to the surface (~100 nm) by TIRF using a 488 nm continuous laser. Inset: side view. (b) Streamline imaging of fluorescently labeled latex beads (1 μm) moving under E-field (1 MHz, 10 V_{pp}) in distilled water. Images represent three consecutive frames (denoted by different colors) superposed and background subtracted to report change in time (SI, Figure S4). Scale bar 100 μm (c) TIRF images of kinetics (time in sec as denoted) of ribosome-GFP attracted and adsorbed near the electrodes by E-field (1 MHz, 10 V_{pp}). Scale bar 50 μm. (d) Measurement of trapping rate in GFP signal (arbitrary units) as a function of applied voltage; arrows denote threshold values, V_{th}, for GFP, ribosome-GFP, and RNAP-GFP, all at equal bulk concentration. (e) Trapping rate as a function of V_{th}^{-2} at applied voltage of 10 V_{pp} (1 MHz).

with either a purified protein fusion of RNAP and GFP (RNAP-GFP), *E. coli* ribosome with a GFP fusion to one of its ribosomal proteins (ribosome-GFP), or GFP alone, each at 0.7 μM concentration (Supporting Information). We imaged these fluorescently labeled molecules using total internal reflection fluorescence (TIRF) microscopy within a ~ 100 nm layer close to the surface between the electrodes. At f = 1 MHz, V = 10 V_{pp} we observed attraction and accumulation of molecules between the electrodes as the TIRF signal increased continuously. Notably, the fluorescent signal between the electrodes, whether of ribosome-GFP, RNAP-GFP or GFP, did not decrease after the E-field had been turned off and stayed at a constant level (shown for RNAP-GFP in Figure S6). Thus, the attracted molecules were most likely adsorbed irreversibly to the surface between the electrodes (Figure 2c). The exact fraction of molecules that were attracted to the surrounding volume around the electrodes but were not adsorbed to the surface could not be determined with the current methodology.

In order to quantitatively evaluate and compare the response of the three different molecules to the E-field, we measured the trapping rate as a function of the applied voltage, and observed an increase in rate with voltage beyond a sharp threshold value V_{th} (Figure 2d, S7). We found a hierarchy in V_{th}, with RNAP-GFP responding at a lower threshold value than both ribosome-GFP and GFP alone (Figure 2d). Using the values of V_{th} we estimated the minimal DEP potential energy $\frac{1}{2}\alpha E_{th}^2$, required to balance the thermal energy, $\frac{3}{2}k_BT$, and calculated the induced polarizability in the reaction solution,[20,34] $\alpha = \frac{3k_BT}{E_{th}^2} \approx \frac{3k_BTd^2}{V_{th}^2} \approx 3.6\cdot10^{-32}$; 2×10^{-32}; 1.4×10^{-32} F·m^2 for RNAP-GFP, ribosome-GFP, and GFP, respectively (Figure 2e). These values are consistent with polarizability values obtained for rRNA,[34] and plasmid DNA[35] at low ionic strength. Furthermore, the trapping rate at 10 V_{pp} increase linearly with V_{th}^{-2} (Figure 2e) for the three different biomolecules, suggesting that DEP is the driving force for trapping, $F_{DEP} = \frac{1}{2}\alpha\nabla E^2 \propto V_{th}^{-2}$, with $F_{DEP} \approx 0$ for small α at which 10 V_{pp} < V_{th}. Finally, molecular attraction near the electrodes is most likely determined by the induced polarizability, and we estimate the order of magnitude of $F_{DEP} \approx \frac{\alpha V^2}{d^3} \approx 10^{-15}N$ (1 MHz, 10 V_{pp}, d = 10 μm). Additional experiments showed that the trapping rate decreased 10-fold as the distance between the electrodes varied from d = 10 to 100 μm (Figure S8), possibly suggesting long-range effects at large electrode distances.

We note that the use of DEP provided us means to measure the high frequency dielectric response of macromolecules under physiological conditions and calculate their induced polarizability α. The induced polarizability depends on the 3D detailed structure of these complex biomolecules, including their chemical composition, charge distribution, molecular weight, and hydrodynamic radius. We could not find a single structural property that intuitively accounts for the observed trend in the response to the DEP force: we found no correlation of the induced polarizability with molecular weight (Figure S9) nor with the charge, as the ribosome is highly charged due to the RNA component, yet its trapping rate was 3-fold lower than that of RNAP. For known biological structures, and given medium the induced polarizability at MHz frequency might be a challenge to compute and is beyond the scope of this work.

We next studied the long-range response of gene expression in DNA brushes during application of an E-field. As a measure of local activity, DNA brushes coding for a nonfluorescent protein under T7 promoter (Supporting Information) were patterned on the surface along the symmetry axis of the E-field, up to 600 μm from the electrodes (Figure 3a). Localized transcription-translation activity was detectable by TIRF[36] as RNAP-GFP, ribosome-GFP, and newly synthesized RNA (labeled by a fluorescent probe[37]), all concentrated at the DNA brush (Figure 3b). Noncoding DNA brushes, symmetrically patterned on the opposite side of the electrodes as background negative controls, did not exhibit localization of RNAP-GFP, RNA or ribosome-GFP (Figure S10). The localized activity at a coding brush, 150 μm from the electrodes, decreased by more than 2-fold relative to a noncoding brush, upon application of the E-field (1 MHz, 10 V_{pp}, for 1 min), with a concomitant accumulation of all the labeled molecules near the electrodes (Figure 2c). As control experiments we measured the direct effect of the E-field on the signals of both immobilized DNA and patterned GFP, and found a minor decrease of ~15−25%, in contrast to the 2-fold effect on diffusible machinery (Figure S11). These experiments

DOI: 10.1021/acssynbio.8b00160
ACS Synth. Biol. 2018, 7, 1829−1833

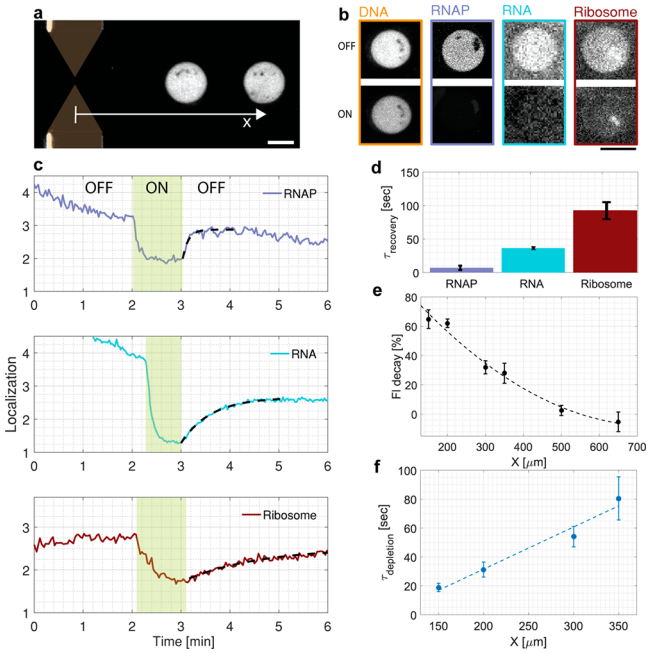

Figure 3. Depletion of biomolecules from DNA brushes undergoing gene expression on the surface. (a) TIRF Image of DNA (end-labeled in red, 647 nm) patterned along *x*-axis from electrodes. Scale bar 50 μm. (b) Imaging transcription-translation activity at DNA brush in separate experiments. Labeled biomolecules during OFF (top) and ON (bottom) states of E-field (1 MHz 10 V_{pp}): DNA, RNAP-GFP, nascent RNA (labeled by broccoli aptamer), and ribosome-GFP; scale bar 50 μm (c) Localization kinetics at DNA brush of RNAP-GFP, synthesized RNA, and ribosome-GFP in response to E-field (turned ON in yellow). Data given in fluorescence fold, $\Delta F = \frac{F_{coding}}{F_{noncoding}}$ of coding to noncoding DNA brushes patterned for reference on opposite side of electrodes ($-x$). (d) Recovery time of RNAP-GFP, nascent RNA and Ribosome-GFP after E-field was turned off, extracted as exponential fits to data (dashed line) in (c). (e) Decay in signal of localized ribosome-GFP after application of E-field, as a function of the distance from the electrodes. (f) Depletion time of ribosome-GFP localized to DNA brush during applied E-field as a function of the distance from the electrodes, extracted by exponential fits to data (c).

demonstrated separation of the enzymatic machinery and synthesized RNA from coding DNA brushes due to attraction toward the electrodes.

The hierarchy in response to the E-field of the biomolecules (Figure 2d,e), together with their different interaction with the DNA brush, motivated us to study the kinetics of depletion and recovery. We observed a rapid 2-fold depletion of RNAP-GFP and ribosome-GFP from the active brush within 20 and 45 s, respectively, after E-field was turned on, followed by localization of molecules from the bulk to the brush within 10 and 90 s, after E-field was turned off (Figure 3c,d). Newly synthesized RNA was also depleted by 2-fold within 20 s and its synthesis recovered over a period of 40 s. Surprisingly, despite the strong direct interaction of RNAP with the DNA, the force induced by the E-field seemed to be pulling it away from the DNA brush more readily than ribosome, possibly due to its higher induced polarizability (Figure 2e). The slower recovery of ribosomes to the brush is likely due to its indirect interaction with DNA coupled to nascent RNA that is bound to RNAP. Consistently with this scenario, the fluorescent signal of newly synthesized RNA was delayed until after the RNAP was localized to the brush (Figure 3c). The effect of the localized E-field on gene-expression activity in a DNA brush was more pronounced closer to the electrodes, as apparent by reduced ribosome localization and faster depletion time in response to the E-field (Figure 3e,f).

In highly conductive aqueous solutions localized E-fields induce Joule heating that generate thermal gradients, resulting in long-range fluid motion.[24,32] To assay the spatial extent and magnitude of this electrothermal effect we immobilized purified GFP molecules on a predetermined pattern in the vicinity of the electrodes and measured their standard epi-fluorescence (insensitive to height) in response to the E-field (Figure S12). We noticed a drop of ∼7% in GFP signal that is consistent with a temperature increase[38] of ∼7 K, which persisted over a scale of ∼250 μm. This suggests that electrothermal effects may lead to the long-range depletion of machinery from DNA brushes.

To summarize, we demonstrated spatiotemporal manipulation by E-field of a cell-free gene expression reaction in a DNA compartment on a chip. Applying strong E-field gradients at MHz frequency offers a new means to attract and trap key components of gene expression at physiologically compatible conditions. The unique scenario of a DNA brush bound to the surface, as the site of transcription-translation, enables spatial separation of the genetic program from the machinery by the localized E-field gradient. We showed that biomolecular machines such as RNAP and ribosome have different induced polarizability, hence can be selectively manipulated by E-field (Figure 2d). For example, at an applied voltage value of 8 V_{pp}, RNAP would be trapped but not ribosomes, opening possibilities for unique modes of gene expression modulations. This result suggests that DEP is the dominant force acting on gene-expression reaction close to the electrodes. Using the values for the estimated polarizability and the simulated E-field (DC) distribution in space (Figure S5) leads to an interaction energy that is weaker than the thermal energy beyond a distance of order $d \sim 10$ μm. Yet, the E-field induced depletion of machinery from DNA brushes occurs at distances of ∼300 μm (Figure 3e). This suggests that long-range flow induced by electrothermal effects entrains biomolecules in the solution, which depletes machinery from the brush. Previous work showed that DEP combined with electrothermal flow resulted in an extended range at which the E-field influenced biomolecule motion,[22,24,25] consistently with our observations. Finally, the assembled biochip can lead to large-scale bioinformation processing systems, which can benefit from the design principles of integrated circuits combined with the powerful capabilities of information processing of biological systems.

■ ASSOCIATED CONTENT

Supporting Information

The Supporting Information is available free of charge on the ACS Publications website at DOI: 10.1021/acssynbio.8b00160.

Description of the numerical model shown in Figure 1e, electric field simulations, extended materials and methods section and additional figures (PDF)

■ AUTHOR INFORMATION

Corresponding Author

*E-mail: roy.bar-ziv@weizmann.ac.il.

ORCID

Roy H. Bar-Ziv: 0000-0002-7583-7900

DOI: 10.1021/acssynbio.8b00160
ACS Synth. Biol. 2018, 7, 1829−1833

Author Contributions

†Y.E. and A.M.T. contributed equally to this work

Notes

The authors declare no competing financial interest.

■ ACKNOWLEDGMENTS

This work was supported by grants from the Israel Science Foundation (grant no. 1870/15), The Minerva Foundation (grant no. 712274), Office of Naval Research (award no. N62909-18-1-2094). A. Tayar thanks the Clore Foundation for a doctoral fellowship.

■ REFERENCES

(1) Basu, S., Gerchman, Y., Collins, C. H., Arnold, F. H., and Weiss, R. (2005) A synthetic multicellular system for programmed pattern formation. *Nature 434*, 1130−4.

(2) Danino, T., Mondragón-Palomino, O., Tsimring, L., and Hasty, J. (2010) A synchronized quorum of genetic clocks. *Nature 463*, 326−30.

(3) Karzbrun, E., Tayar, A. M. A. M., Noireaux, V., and Bar-Ziv, R. H. R. H. (2014) Programmable on-chip DNA compartments as artificial cells. *Science 345*, 829−832.

(4) Tayar, A. M., Karzbrun, E., Noireaux, V., and Bar-Ziv, R. H. (2017) Synchrony and pattern formation of coupled genetic oscillators on a chip of artificial cells. *Proc. Natl. Acad. Sci. U. S. A. 114*, 11609−11614.

(5) Haellman, V., and Fussenegger, M. (2017) Synthetic biology − Engineering cell-based biomedical devices. *Curr. Opin. Biomed. Eng. 4*, 50−56.

(6) Brophy, J. A. N., and Voigt, C. A. (2014) Principles of genetic circuit design. *Nat. Methods 11*, 508−20.

(7) Daniel, R., Rubens, J. R., Sarpeshkar, R., and Lu, T. K. (2013) Synthetic analog computation in living cells. *Nature 497*, 619−23.

(8) Deiters, A. (2009) Light activation as a method of regulating and studying gene expression. *Curr. Opin. Chem. Biol. 13*, 678−686.

(9) Levskaya, A., Weiner, O. D., Lim, W. A., and Voigt, C. A. (2009) Spatiotemporal control of cell signalling using a light-switchable protein interaction. *Nature 461*, 997−1001.

(10) Booth, M. J., Schild, V. R., Graham, A. D., Olof, S. N., and Bayley, H. (2016) Light-activated communication in synthetic tissues. *Sci. Adv. 2*, e1600056.

(11) Mannix, R. J., Kumar, S., Cassiola, F., Montoya-Zavala, M., Feinstein, E., Prentiss, M., and Ingber, D. E. (2008) Nanomagnetic actuation of receptor-mediated signal transduction. *Nat. Nanotechnol. 3*, 36−40.

(12) Dobson, J. (2008) Remote control of cellular behaviour with magnetic nanoparticles. *Nat. Nanotechnol. 3*, 139−143.

(13) Gordonov, T., Kim, E., Cheng, Y., Ben-Yoav, H., Ghodssi, R., Rubloff, G., Yin, J.-J., Payne, G. F., and Bentley, W. E. (2014) Electronic modulation of biochemical signal generation. *Nat. Nanotechnol. 9*, 605−610.

(14) Tschirhart, T., Kim, E., McKay, R., Ueda, H., Wu, H.-C., Pottash, A. E., Zargar, A., Negrete, A., Shiloach, J., Payne, G. F., and Bentley, W. E. (2017) Electronic control of gene expression and cell behaviour in Escherichia coli through redox signalling. *Nat. Commun. 8*, 14030.

(15) Shivashankar, G. V., Liu, S., and Libchaber, A. (2000) Control of the expression of anchored genes using micron scale heater. *Appl. Phys. Lett. 76*, 3638.

(16) Kreysing, M., Keil, L., Lanzmich, S., and Braun, D. (2015) Heat flux across an open pore enables the continuous replication and selection of oligonucleotides towards increasing length. *Nat. Chem. 7*, 203−208.

(17) Bazant, M. Z., Thornton, K., and Ajdari, A. (2004) Diffuse-charge dynamics in electrochemical systems. *Phys. Rev. E 70*, 21506.

(18) Pohl, H. A. (1978) *Dielectrophoresis: The Behavior of Neutral Matter in Nonuniform Electric Fields*, Cambridge University Press.

(19) Nakano, A., and Ros, A. (2013) Protein dielectrophoresis: Advances, challenges, and applications. *Electrophoresis 34*, 1085−1096.

(20) Tuukkanen, S., Kuzyk, A., Toppari, J. J., Häkkinen, H., Hytönen, V. P., Niskanen, E., Rinkiö, M., and Törmä, P. (2007) Trapping of 27 bp−8 kbp DNA and immobilization of thiol-modified DNA using dielectrophoresis. *Nanotechnology 18*, 295204.

(21) Hölzel, R., Calander, N., Chiragwandi, Z., Willander, M., and Bier, F. F. (2005) Trapping Single Molecules by Dielectrophoresis. *Phys. Rev. Lett. 95*, 128102.

(22) Castellanos, A., Ramos, A., González, A., Green, N. G., and Morgan, H. (2003) Electrohydrodynamics and dielectrophoresis in microsystems: scaling laws. *J. Phys. D: Appl. Phys. 36*, 2584−2597.

(23) Nili, H., and Green, N. G. (2015) AC Electrokinetics of Nanoparticles, in *Encyclopedia of Nanotechnology*, pp 1−10, Springer Netherlands, Dordrecht.

(24) Chaurey, V., Polanco, C., Chou, C.-F., and Swami, N. S. (2012) Floating-electrode enhanced constriction dielectrophoresis for bio-molecular trapping in physiological media of high conductivity. *Biomicrofluidics 6*, 12806.

(25) Gao, J., Sin, M. L. Y., Liu, T., Gau, V., Liao, J. C., and Wong, P. K. (2011) Hybrid electrokinetic manipulation in high-conductivity media. *Lab Chip 11*, 1770−5.

(26) Shimizu, Y., Inoue, A., Tomari, Y., Suzuki, T., Yokogawa, T., Nishikawa, K., and Ueda, T. (2001) Cell-free translation reconstituted with purified components. *Nat. Biotechnol. 19*, 751−755.

(27) Noireaux, V., Bar-Ziv, R., and Libchaber, A. (2003) Principles of cell-free genetic circuit assembly. *Proc. Natl. Acad. Sci. U. S. A. 100*, 12672−12677.

(28) Shin, J., and Noireaux, V. (2012) An E. coli cell-free expression toolbox: application to synthetic gene circuits and artificial cells. *ACS Synth. Biol. 1*, 29−41.

(29) Noireaux, V., and Libchaber, A. (2004) A vesicle bioreactor as a step toward an artificial cell assembly. *Proc. Natl. Acad. Sci. U. S. A. 101*, 17669−74.

(30) Niederholtmeyer, H., Stepanova, V., and Maerkl, S. J. (2013) Implementation of cell-free biological networks at steady state. *Proc. Natl. Acad. Sci. U. S. A. 110*, 15985−90.

(31) Hansen, M. M. K., Meijer, L. H. H., Spruijt, E., Maas, R. J. M., Rosquelles, M. V., Groen, J., Heus, H. A., and Huck, W. T. S. (2016) Macromolecular crowding creates heterogeneous environments of gene expression in picolitre droplets. *Nat. Nanotechnol. 11*, 191−197.

(32) Morgan, H., and Green, N. G. (2003) *AC Electrokinetics: Colloids and Nanoparticles*, Research Studies Press.

(33) Ermolina, I., and Morgan, H. (2005) The electrokinetic properties of latex particles: comparison of electrophoresis and dielectrophoresis. *J. Colloid Interface Sci. 285*, 419−428.

(34) Giraud, G., Pethig, R., Schulze, H., Henihan, G., Terry, J. G., Menachery, A., Ciani, I., Corrigan, D., Campbell, C. J., Mount, A. R., Ghazal, P., Walton, A. J., Crain, J., and Bachmann, T. T. (2011) Dielectrophoretic manipulation of ribosomal RNA. *Biomicrofluidics 5*, 24116.

(35) Suzuki, S., Yamanashi, T., Tazawa, S., Kurosawa, O., and Washizu, M. (1998) Quantitative analysis of DNA orientation in stationary AC electric fields using fluorescence anisotropy. *IEEE Trans. Ind. Appl. 34*, 75−83.

(36) Bracha, D., Karzbrun, E., Daube, S. S., and Bar-Ziv, R. H. (2014) Emergent Properties of Dense DNA Phases toward Artificial Biosystems on a Surface. *Acc. Chem. Res. 47*, 1912−1921.

(37) Filonov, G. S., Moon, J. D., Svensen, N., and Jaffrey, S. R. (2014) Broccoli: Rapid Selection of an RNA Mimic of Green Fluorescent Protein by Fluorescence-Based Selection and Directed Evolution. *J. Am. Chem. Soc. 136*, 16299−16308.

(38) Nakano, M., Arai, Y., Kotera, I., Okabe, K., Kamei, Y., Nagai, T., and Matsumoto, T. (2017) Genetically encoded ratiometric fluorescent thermometer with wide range and rapid response. *PLoS One 12*, e0172344.

DOI: 10.1021/acssynbio.8b00160
ACS Synth. Biol. 2018, 7, 1829−1833